Rotating spirals in a Faraday experiment

S. V. Kiyashko,[1] L. N. Korzinov,[1,2] M. I. Rabinovich,[1,2] and L. S. Tsimring[2]
[1]*Institute of Applied Physics, Russian Academy of Science, Nizhni Novgorod, 603600, Russia*
[2]*Institute for Nonlinear Science, University of California, San Diego, La Jolla, California 92093-0402*
(Received 6 February 1996)

We report experiments and model simulations of patterns of parametrically excited capillary ripples in a large aspect-ratio cell with thin horizontal layer of viscous fluid subjected to sinusoidal vertical oscillations. We found stable rotating spirals with different topological charges in the parameter range where steady straight rolls were observed previously. Formation of multiarmed spirals via dislocations approaching a target core was observed. The direction of the spiral rotation depends on its chirality and is always consistent with wave propagation towards the core. Wave drift towards the spiral core is associated with the shear flow which is generated near the walls by rapidly decaying viscous surface waves. [S1063-651X(96)02911-X]

PACS number(s): 47.54.+r, 47.35.+i

Capillary ripples parametrically excited by an oscillating gravity field (Faraday experiment [1]) is a very convenient and popular wave system for understanding of many pattern formation phenomena, including temporal [2] and spatiotemporal chaos [3,4], formation of crystalline [4–6] and quasicrystalline surface patterns [5,7], and defect dynamics [8–10].

In this paper we report results of experimental and numerical study of stationary rotating spirals, targets, and defects in a large aspect-ratio system [$\Gamma=$(diameter)/(height)$\simeq 30$]. One aspect of wave patterns in Faraday experiment that distinguishes them from patterns in other wave systems (autocatalytic chemical reactions [11,12], Rayleigh-Bénard convection in binary fluids [13,14], neuronlike media [15]) is that they are composed of pairs of counterpropagating waves. In systems with reflection symmetry, they have equal frequencies (half of the fundamental frequency) and opposite wave vectors. The sum of the phases of these waves is conserved in the whole space and is equal to the phase of the homogeneous oscillating pumping field. Therefore the only ''allowed'' patterns of capillary ripples appear to be standing waves or superposition of several standing waves. Various patterns of this type were observed in Faraday experiment in different parameter regions [4–6]. Nevertheless, our present findings demonstrate the unexpected phenomenon: under certain conditions, patterns of slowly drifting standing waves arise, such as rotating spirals and contracting targets. These patterns appear within a parameter range where plane standing waves are stationary. Independent of the chirality of the spiral, waves always drift towards the core. We argue that the mechanism of this slow drift is associated with small near-wall shear flow which near the surface is always directed away from the wall. It is induced by a surface wave at the fundamental frequency excited by the oscillating meniscus [16]. This high-frequency wave decays rapidly off the wall and transforms its momentum into the shear flow. This flow is observed even below the threshold of parametrical instability. The shear flow is localized near the walls of the cell, however, it affects the bulk of the cell by sending additional ''rolls'' and therefore moving the wave number away from its selected value at a given frequency (''wave-vector frustration''). The frustrated pattern tries to restore its wave number by eliminating a roll which is near the core of the spiral (or target), after which the process repeats. This mechanism is somewhat similar to the mechanism of generating traveling axisymmetric rolls in small aspect-ratio system [17] and rotating spirals [18] in large aspect-ratio Rayleigh-Bénard convection in Boussinesq fluid. In both cases a driving force for roll motion is the wave number frustration because the boundary selects the wave number differing from the wave number selected by the core of a spiral or target. In our case, the boundary serves as a phase source, near-wall shear flow ''squeezes'' waves in the bulk by sending in additional waves, and therefore frustrates the wave number which is selected by the parametric instability at a given pumping frequency. The qualitative features of the process do not depend on the form of the cavity—we observed spiral rotation and target contraction in both round and square cells.

The scheme of the experiment is described in detail in [10]. Measurements were performed in a round cell 16 cm in diameter and in a square cell with side 11 cm. General survey of various patterns was carried out in either a mixture of glycerol and water or silicon oils with different viscosities (from $\nu=0.05\text{cm}^2/\text{sec}$ to $\nu=2.0\text{cm}^2/\text{sec}$). The depth of the layer varied between 0.3 and 1 cm, the pumping frequency varied from 10 to 180 Hz. Detailed studies of spirals and targets were performed using silicon oil with viscosity $\nu=1.0\text{cm}^2/\text{sec}$, density $\rho=0.97\text{g/cm}^3$, and surface tension coefficient $\sigma=20.5$ dyn/cm (all of the data are given for the temperature of 20 °C). The depth of the liquid layer was $h=0.5$ cm, and the wavelength of the patterns is $\lambda=0.85$ cm (pumping frequency $f_0=56$ Hz). For small enough viscosity and large $h\lambda^{-1}$ square patterns are observed [3], for smaller $h\lambda^{-1}$ hexagons appear (see also [6]). For large $h\lambda^{-1}$ and ν, depending on initial conditions, either standing plane waves or targets and spirals could be observed. The crossover from squares to stripes due to increasing viscosity of fluid was also observed by Daudet *et al.* [19], however, they did not observe targets and spirals.

As we mentioned earlier, whereas plane standing waves are completely stationary (nodes and antinodes do not move), standing waves forming targets and spirals drift slowly toward the core. The speed of the drift depends

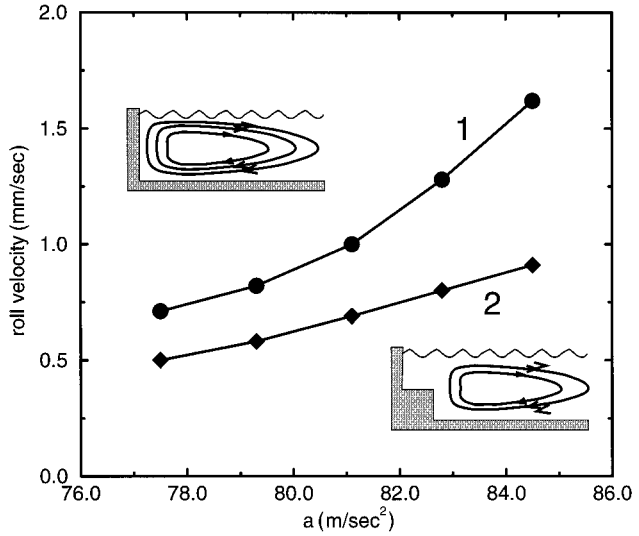

FIG. 1. Velocity of wave drift (measured by node displacement) as a function of magnitude of vertical acceleration for two different profiles of side walls. Inset: Sketches of the vertical profiles of the side wall and the structure of the shear flow.

strongly on the magnitude of vertical oscillations, as shown in Fig. 1. On the other hand, wave drift phase velocity depends sensitively on the profile of the side walls of the cell. The drift velocity is maximal for a straight vertical wall, and is reduced for an oblique wall and a wall with a step. We hypothesize that the wave drift is related to a shear flow produced near the wall by rapidly decaying surface waves at the fundamental frequency, generated by an oscillating meniscus. This shear flow is indeed observed even in the subcritical regime when the parametrical instability was absent. Near the threshold, the magnitude of velocity of the shear flow was ≈ 0.5 mm/sec. The vertical structure of the flow near the wall is sketched in the insets to Fig. 1. Clearly, the average mass transport through any azimuthal cross section of the cell must be zero in stationary conditions and therefore off-wall flow near the surface is compensated by a reverse flow near the bottom. However, since waves are localized near the surface, the near-surface part of the flow is more essential for wave drift than the near-bottom part. Both contracting targets and rotating multiarmed spirals persisted for a long time (a few hours) in the cavity.

Multiarmed spirals with different values of topological charge emerge as a result of dislocations interacting with the background target pattern. Dislocation pairs can be easily produced by perturbing rolls at the periphery of the target. One dislocation of the pair quickly disappears at the wall, and another moves towards the center along some curved trajectory (see Fig. 2). Which dislocation moves to the wall, and which to the center, depends on details of initial perturbation, and varied from event to event, so spirals of different chirality could be produced. The velocity of the defect increases as it approaches the core. This phenomenon is qualitatively similar to the interaction of dislocations with targets in convective patterns at low Prandl number [20,13]. When we introduce the several defects on the target we observed stable multiarmed spirals with topological charge ranging from 1 to 7. In Fig. 2 the evolution of a target with four dislocations (two positive and two negative) is shown. A

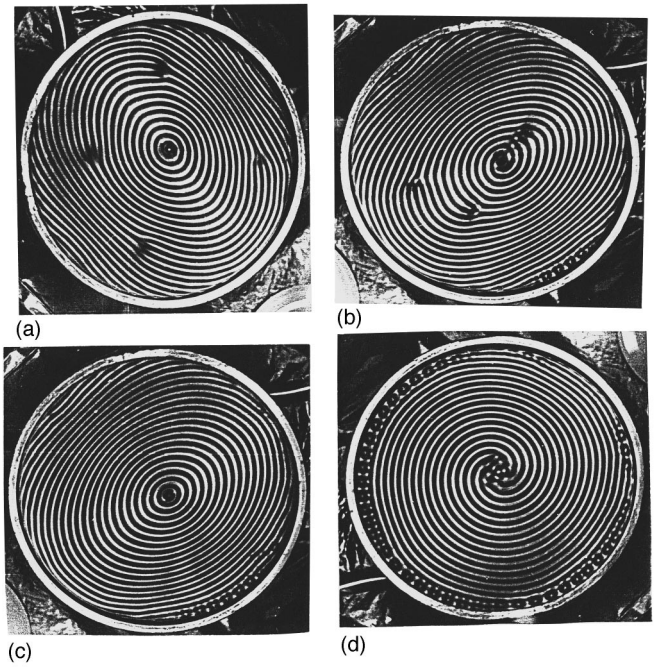

FIG. 2. Series of snapshots of Faraday ripples in laboratory experiment: (a)—a target with four dislocations (two positive and two negative); (b)—one dislocation is attracted to the target core, spiral is formed; (c)—all dislocations have been attracted to the center and annihilated, perfect target reappeared; (a), (b), and (c) are separated by 2.0 sec; (d)—asymptotic state of another experiment where a three-armed spiral was formed and rotated for a long time (one period of a standing wave corresponds to two white and two dark stripes on the photos due to time averaging).

spiral is formed when one of the defects is already at the center while the others are still on the periphery [Fig. 2(b)], and later [Fig. 2(c)] a target is restored when all the dislocations annihilate at the center. In another experiment, a two-armed spiral was formed and persisted for a long time [Fig. 2(d)].

We have investigated numerically phenomena described above within the model equation for the complex order parameter $\psi(\mathbf{r},t)$ which is introduced as follows:

$$\xi(\mathbf{r},t)=\psi(\mathbf{r},t)\exp(i\omega_0 t)+\overline{\psi}(\mathbf{r},t)\exp(-i\omega_0 t). \qquad (1)$$

Here $\xi(\mathbf{r},t)$ is instantaneous deviation of the fluid surface, $\psi(\mathbf{r},t)$ is the slowly varying in time amplitude of the parametrically excited capillary patterns ($2\omega_0$ is the forcing frequency), and the bar refers to the complex conjugate. With this choice of the complex order parameter, we eliminate fast temporal oscillations, but retain the spatial structure of patterns unconstrained, which enables us to study different geometrical configurations of capillary ripples within the framework of one model equation.

The model equation, which incorporates basic features of parametrical instability, dispersion of surface capillary waves, viscous dissipation, and nonlinearity can be written in the following form:

$$\frac{\partial\psi}{\partial t}=i\gamma\overline{\psi}-\nu\nabla^2\psi-(1+i\alpha)|\psi|^2\psi+i\kappa(\nabla^2+k_0^2)\psi$$
$$-(\mathbf{u}\cdot\nabla)\psi. \qquad (2)$$

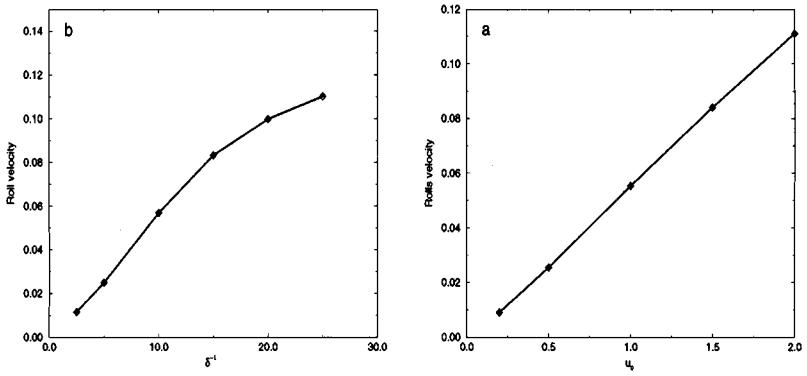

FIG. 3. Phase velocity of waves as a function of shear flow magnitude u_0 (a) and inverse scale ξ (b) from numerical simulations of (2). Parameters of simulations: $\gamma=1.0, \nu=0.5, \alpha=0.0$, $\kappa=1.0, k_0=1, \xi=0.1$. In (a), $\xi=0.1$, in (b), $u_0=1.0$.

Here γ is a forcing magnitude, κ is the dispersion parameter, and $\mathbf{u}$ is the velocity of the shear flow weighted with the surface wave vertical mode distribution. Linear terms in this equation can be derived from the dispersion relation for capillary waves under parametric excitation, expanded near $\omega=\omega_0, k=k_0$. The dispersion relation for free capillary waves in nondimensional form reads $\omega^2=k^3$, therefore $k_0=\omega_0^{2/3}$, $\kappa=3\omega_0/4k_0^2$. The nonlinear term cannot be derived rigorously, as in other Swift-Hohenberg type models, and has been added *ad hoc* to account for stabilization of the parametric instability. The imaginary part of nonlinear coefficient α describes nonlinear frequency shift (see also [21]). The last term in the right-hand side of Eq. (2) describes shear flow transport near the walls of the cavity.

Equation (2) with periodic boundary conditions was studied numerically using a pseudospectral split-step method with 256×256 collocation points, domain size $d=200$, and integration time step 0.05. To simulate waves in a circular cavity, we ramped linear dissipation outside the circle of radius $r_0=86$, i.e., $\nu=\nu_0, r<r_0$ and $\nu=\nu_0[1+k(r-r_0)], r>r_0$, where k varied between 0.5 and 1.0.

For $\gamma>\mu$ trivial state $\psi=0$ is unstable with respect to perturbations with wave numbers near k_0. Numerical simulations show that at the nonlinear stage, these perturbations give rise to various cellular patterns, including plane waves, targets, and spirals. Without the shear flow term ($\mathbf{u}\equiv\mathbf{0}$), these patterns remain stationary even when nonlinear coefficients in (2) are complex. Nonlinear frequency shift $\propto\alpha$ only leads to deviation of the selected wave number from $k=k_0$. [In systems with ordinary (nonparametric) pattern-forming instabilities any nonpotential effect leads to wave propagation.] However, when near-wall shear flow is introduced in (2), targets and spirals begin to drift slowly toward the center.

We assumed that the flow had radial direction and was azimuthally symmetric, $\mathbf{u}=u(r)\hat{\mathbf{r}}$. We used the following profile for flow velocity $u(r)$:

$$u(r)=u_0\exp[\xi(r-r_0)] \tag{3}$$

and measured rolls velocity for different ξ and u_0. Note that $\xi\gg r_0^{-1}$ so the shear flow is absent in the bulk, still rolls are moving throughout the integration domain. The results of velocity calculations are presented in Fig. 3. We observe that the phase velocity of rolls grows linearly with u_0 as should be expected. We also tried different stepwise profiles of radial velocity as a function of r; the qualitative behavior of patterns is not sensitive to the particular choice of the profile.

In computer simulations we also observed spiral formation via dislocation motion to the core of a target. When several dislocations are placed on the target, they all are attracted to the center, and a multiarmed spiral is formed with the topological charge equal to a sum of topological charges of dislocations. Several snapshots of dislocation motion are shown in Fig. 4. Dislocation motion is independent of wave propagation: dislocation usually moves faster than rolls and is attracted to the core even when shear flow is absent and a target is stationary.

The mechanism of dislocation motion can be elucidated using the phase approximation for Eq. (2) with $\alpha=0$. Far from the cores of target and dislocation, the complex order parameter can be written in the form

$$\psi(r,t)=[A(r)+\delta a_+]\exp(ik_0r+i\phi_+)+i[A(r)+\delta a_-]\times\exp(-ik_0r+i\phi_-), \tag{4}$$

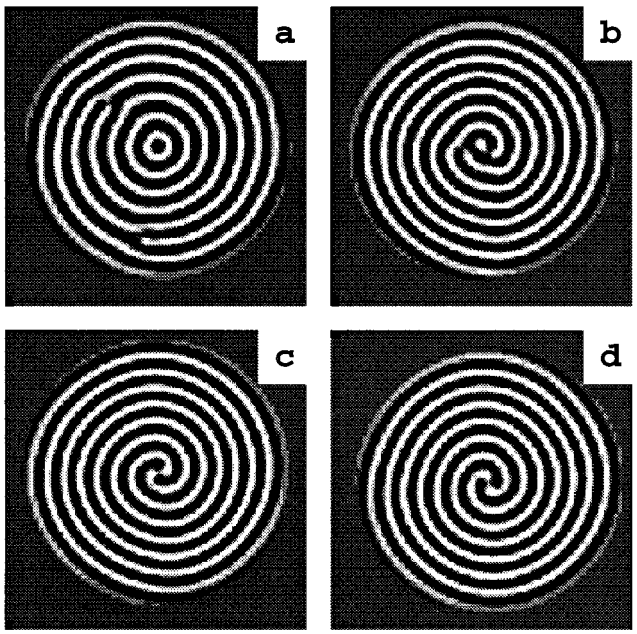

FIG. 4. Snapshots of multiarmed spiral formation in numerical simulation. A target with two dislocations on periphery was taken as initial condition, parameters of the models are given in the caption to Fig. 3; (a) $t=10$; (b) $t=100$; (c) $t=200$; (d) $t=300$. Spiral rotation is obvious from comparison of (c) and (d).

where $A(r)=\sqrt{\gamma-\nu k_0^2-\kappa k_0/r^2}$ with the accuracy $O(r^{-2})$. Substitution of (4) into (2) and eliminating the amplitude perturbation $\delta a_{\pm}$ in the first approximation yields two coupled phase equations

$$\frac{\partial\phi_+}{\partial t}=-\gamma\sin(\phi_++\phi_-)+\kappa k_0\frac{\partial\phi_+}{\partial r}+\nu\left(\frac{\partial^2\phi_+}{\partial r^2}+\frac{1}{r}\frac{\partial\phi_+}{\partial r}\right), \tag{5}$$

$$\frac{\partial\phi_-}{\partial t}=-\gamma\sin(\phi_++\phi_-)-\kappa k_0\frac{\partial\phi_-}{\partial r}+\nu\left(\frac{\partial^2\phi_-}{\partial r^2}+\frac{1}{r}\frac{\partial\phi_-}{\partial r}\right). \tag{6}$$

In the limit of strong parametric coupling of counterpropagating waves, the sum of phases $\Phi=\phi_++\phi_-$ is small and follows adiabatically slow variations of phase difference $\Delta=\phi_+-\phi_-$ far from the cores of the target and dislocations. This allows one to eliminate Φ and obtain one equation for Δ,

$$\frac{\partial\Delta}{\partial t}=\left(\frac{\kappa^2k_0^2}{2\gamma}+\nu\right)\frac{\partial^2\Delta}{\partial r^2}+\frac{\nu}{r}\frac{\partial\Delta}{\partial r}. \tag{7}$$

Although this equation is not exactly variational, for strong parametric coupling it becomes variational with potential $F[\Delta]=\nu\int\Delta_r^2 r\,dr$. In this limit it is equivalent to the variational phase equation for large scale phase perturbations of target patterns deduced from the Swift-Hohenberg equation (see [22]). In [22] it was shown that a dislocation experiences a Peach-Koehler type force directed perpendicular to the curved rolls which is inversely proportional to the distance from the center. This force leads to dislocation gliding towards the core of a target. The same effect takes place for dislocation in parametrically excited standing waves.

In summary, we investigated pattern formation in a Faraday experiment in a large aspect-ratio container. In the parameter range corresponding to standing straight rolls, we discovered multiarmed rotating spiral waves. Spirals were formed from a target pattern after a dislocation pair was created near the side wall. One of the dislocations quickly disappears on the wall, and another moves towards the center, and eventually a single-armed spiral is formed. If several dislocations are produced, a multiarmed spiral appears. Spiral rotation is caused by a near-wall shear flow directed towards the center of the cell. This shear flow is produced by decaying surface capillary waves at the fundamental frequency which are generated by oscillating meniscus. The near-wall shear flow provides wave-vector frustration in the bulk, which in turn drives the waves towards the center. We reproduced this scenario in numerical simulations with our phenomenological model Eq. (2) which describes parametrically excited waves in rotationally invariant system.

We acknowledge support from the U.S. Department of Energy (Grants No. DE-FG03-95ER14516 and No. DE-FG03-96ER14592), International Science Foundation (Grants No. NOU 000 and No. NOU 300), and Russian Fundamental Research Foundation (Grant No. 06-05-64551).

[1] M. Faraday, Philos. Trans. R. Soc. London, Ser. A **52**, 299 (1831).
[2] S. Ciliberto and J.P. Gollub, Phys. Rev. Lett. **52**, 922 (1984); R. Keolian, L.A. Turkevich, S.J. Putterman, I. Rudnik, and J.A. Rudnik, *ibid.* **47**, 1133 (1981).
[3] A.B. Ezersky, P.I. Korotin, and M.I. Rabinovich, Pis'ma Zh. Éksp. Teor. Fiz. **41**, 4 (1985) [JETP Lett. **41**, 157 (1985)]; N.B. Tufillaro, R. Ramshankar, and J.P. Gollub, Phys. Rev. Lett. **62**, 422 (1989).
[4] A.B. Ezersky, M.I. Rabinovich, V.P. Reutov, and I.M. Starobinets, Zh. Éksp. Teor. Fiz. **91**, 2070 (1986) [Sov. Phys. JETP **64**, 1228 (1986)].
[5] W.S. Edwards and S. Fauve, J. Fluid Mech. **278**, 123 (1994).
[6] K. Kumar and K.M.S. Bajaj, Phys. Rev. E **52**, R4606 (1995).
[7] B. Christiansen, P. Alstrom, and M.T. Levinsen, Phys. Rev. Lett. **68**, 2157 (1992).
[8] M.C. Cross and P. Hohenberg, Rev. Mod. Phys. **65**, 851 (1993).
[9] A.V. Gaponov-Grekhov and M.I. Rabinovich, Phys. Today **43**(7), 30 (1990); A.B. Ezersky, S.V. Kiyashko, P.A. Matusov, and M.I. Rabinovich, Europhys. Lett. **26**, 183 (1994).
[10] A.B. Ezersky, D.A. Ermoshin, and S.V. Kiyashko, Phys. Rev. E **51**, 441 (1995).
[11] D.A. Kessler and H. Levine, Physica D **39**, 1 (1989).
[12] G.S. Skinner and H.L. Swinney, Physica D **48**, 1 (1991).
[13] J.J. Niemela, G. Ahlers, and D.S. Cannel, Phys. Rev. Lett. **64**, 1365 (1990).
[14] D.R. Ohlsen, S.Y. Yamamoto, C.M. Surko, and P. Kolodner, Phys. Rev. Lett. **65**, 1431 (1990).
[15] J.G. Milton, P.H. Chu, and J.D. Cowan, in *Neural Information Processing Systems 5*, edited by S.J. Hanson, J.D. Cowan, and J.L. Giles (Morgan Kaufmann Publishers, San Mateo, 1995), p. 1001.
[16] S. Douady, J. Fluid Mech. **221**, 383 (1990).
[17] D. Barkley and L.S. Tuckerman, Physica D **37**, 288 (1989).
[18] M.C. Cross and Y. Tu., Phys. Rev. Lett. **75**, 834 (1995).
[19] L. Daudet, V. Ego, S. Manneville, and J. Bechhoefer, Europhys. Lett. **32**, 313 (1995).
[20] V. Croquette, Contemp. Phys. **30**, 153 (1989).
[21] W. Zhang and J. Vinals, Phys. Rev. E **74**, 690 (1995).
[22] A.S. Nikulin, L.N. Korzinov, and M.I. Rabinovich, Phys. Lett. A **177**, 421 (1993).